Renewable Energy 71 (2014) 166–175

Contents lists available at ScienceDirect

Renewable Energy

journal homepage: www.elsevier.com/locate/renene

Nonlinear system identification for model-based condition monitoring of wind turbines

Philip Cross*, Xiandong Ma

Engineering Department, Lancaster University, Lancaster LA1 4YR, United Kingdom

ARTICLE INFO

Article history:
Received 4 June 2013
Accepted 16 May 2014
Available online

Keywords:
Distributed generation (DG)
Wind turbine
Condition monitoring (CM)
Fault detection
Modelling and simulation
SCADA data

ABSTRACT

This paper proposes a data driven model-based condition monitoring scheme that is applied to wind turbines. The scheme is based upon a non-linear data-based modelling approach in which the model parameters vary as functions of the system variables. The model structure and parameters are identified directly from the input and output data of the process. The proposed method is demonstrated with data obtained from a simulation of a grid-connected wind turbine where it is used to detect grid and power electronic faults. The method is evaluated further with SCADA data obtained from an operational wind farm where it is employed to identify gearbox and generator faults. In contrast to artificial intelligence methods, such as artificial neural network-based models, the method employed in this paper provides a parametrically efficient representation of non-linear processes. Consequently, it is relatively straightforward to implement the proposed model-based method on-line using a field-programmable gate array.

1. Introduction

Recently, there has been increasing interest in the distributed generation (DG) of electricity due to the deregulation of utilities, environmental constraints, and concerns regarding climate change [1]. In the context of this paper, DG refers to electric power generation sources connected directly to the distribution network allowing for the integration of renewable energy resources, such as solar, CHP (Combined Heat and Power), and wind [2], with capacities ranging from less than 1 kW to over 100 MW.

The potential benefits of using DG include a more reliable electrical power supply and power loss reduction over transmission lines by generating electricity closer to the end user. Indeed, DG can provide power with little reliance on the grid. However, DG systems present several problems. Conventionally, voltage and reactive power control is based upon on the assumption that power flows from a generator to a substation, and subsequently to the feeders. The introduction of DG systems alters this power flow, causing problems with voltage regulation, equipment ratings to be exceeded, and protection schemes to be misdirected [3]. Consequently, it is vital for DG systems to operate reliably, and health condition monitoring and diagnostics schemes are essential.

Wind turbines represent a major form of distributed generation. It is common for wind turbines to be installed in remote locations on land or offshore, leading to difficulties in routine inspection and maintenance. In addition, wind turbines in these locations are often subject to harsh operating conditions. Over an operating life of 20 years, the maintenance costs for an offshore wind farm are estimated to be up to 30% of the total income [4]. Therefore, condition monitoring (CM) systems play an important role in the reliable operation of wind farms, providing information about the past and current condition of wind turbines and enabling optimal scheduling of maintenance activities, while minimising the risk of unexpected failure.

Given known input signals of a process, the corresponding output signals can be predicted using models obtained from the data generated by a monitoring system, such as SCADA (Supervisory Control and Data Acquisition) [5], and a CM scheme can be implemented by comparing actual output data with that predicted by the model. Any differences between the measurement and prediction signals could be caused by changes in the process, possibly due to the occurrence of faults [6]. The model-based method is illustrated in Fig. 1, in which the residual signal can reveal potential component failures. Clearly, an accurate model is essential for such a scheme, and previous research has employed a range of modelling techniques.

Mechanistic modelling techniques, for example using software such as Simulink [7], require a thorough understanding of the process, and may result in a complex or over-parameterised model

* Corresponding author. University of Leeds, Leeds LS2 9JT, United Kingdom. Tel.: +44 (0) 1524 593700.
E-mail addresses: p.cross@leeds.ac.uk (P. Cross), xiandong.ma@lancaster.ac.uk (X. Ma).

http://dx.doi.org/10.1016/j.renene.2014.05.035
0960-1481/

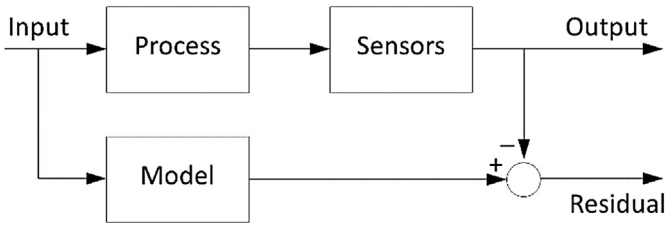

Fig. 1. Schematic diagram of the model-based condition monitoring system.

not suitable for on-line implementation as a CM system. Data-based models [8] do not require knowledge of the process or specific parameters, they are obtained directly from measured input and output signals collected either during planned experiments or by monitoring the process during normal operation. When implementing a CM scheme on-line using data-based models, it is essential to identify a low-order model. Higher-order models require increasingly more values of the past input and output signals to calculate the predicted output, resulting in an increased response time.

Many processes associated with wind turbines are non-linear. Artificial intelligence (AI) techniques are utilised by many researchers for model-based CM schemes, for example artificial neural networks (ANNs) [9] and fuzzy logic [10]. AI techniques are particularly suitable for this application being robust to noisy, incomplete and uncertain data. It should be noted that care needs to be taken to avoid 'over-fitting' of an ANN to the training data, which can lead to a poor performance when implemented on-line.

This paper proposes a non-linear data-based modelling approach to condition monitoring in which the model parameters vary as functions of the system variables, or 'state variables' [11]. The model structure and the model parameters are identified directly from the input and output data of the process. Although these state dependent parameter models cannot represent every type of non-linear behaviour, they are applicable to a wide range of processes, including those that behave chaotically. In contrast to ANNs, the data-based models employed in this paper are a parametrically efficient representation of non-linear processes, and are particularly suitable for forecasting [12], and providing the basis for automatic controller design [13]. However, the research described here represents the first occasion for which this type of model has been employed for a CM system.

The remainder of this paper is organised as follows. Section 2 describes the system identification methodology used in the research. A computer simulation of a grid-connected wind turbine is described in Section 3. Grid and power electronics faults are included in the simulation, and the non-linear model-based CM method is demonstrated by identifying these faults. In Section 4, non-linear models of an operational turbine are obtained using fault-free SCADA data, which are used to identify gearbox and generator faults in turbines on the same farm. Adaptive thresholds are derived from the model predictions, which in turn form the basis of an early warning system. A hardware implementation of the proposed approach, using an FPGA (field-programmable gate array), is presented in Section 5. Finally, conclusions to the research and future work are discussed in Section 6.

2. Model identification

A linear system can be represented by an auto-regressive with exogenous variables (ARX) model or auto-regressive moving average with exogenous variables (ARMAX) model. These model structures are usually represented by a discrete-time transfer function model, describing the relationship between the input and output signals as a ratio of polynomials. However, many processes associated with wind turbines are non-linear, and, although linear models can predict the output of many non-linear processes over a small operating range, this may be inadequate for model-based CM systems. In this regard, non-linear ARX models based upon ANNs have been utilised for wind turbine fault detection [9].

In this paper, non-linear processes are modelled using the following dynamic auto-regressive exogenous (DARX) model, in which the identified non-linearity is characterised by the time varying model parameters,

$$y_k = \frac{B(z^{-1},k)}{A(z^{-1},k)}u_k + \frac{1}{A(z^{-1},k)}e_k \tag{1}$$

where y_k and u_k are the kth sampled output and input variables respectively; e_k is white noise with zero mean and variance σ^2 that accounts for any random component of the observed data; $A(z^{-1},k)$ and $B(z^{-1},k)$ are appropriately defined polynomials in the backward shift operator, z^{-1},

$$A\left(z^{-1},k\right) = A\left(\boldsymbol{\chi}_{1,k},z^{-1}\right) = 1 + a_1(\chi_{11,k})z^{-1} + \cdots + a_n(\chi_{1n,k})z^{-n}$$

$$B\left(z^{-1},k\right) = B\left(\boldsymbol{\chi}_{1,k},z^{-1}\right) = b_0(\chi_{21,k}) + b_1(\chi_{22,k})z^{-1} + \cdots + b_m(\chi_{2m,k})z^{-m} \tag{2}$$

in which the model parameters, $a_1 \ldots a_n$, $b_0 \ldots b_m$, are non-linear functions of the vectors $\boldsymbol{\chi}_{1,k} = [\chi_{11} \cdots \chi_{1n}]$ and $\boldsymbol{\chi}_{2,k} = [\chi_{21} \cdots \chi_{2m}]$ defined in terms of the system variables, or 'state variables', upon which the parameters are dependent. A time delay of δ samples is incorporated into the model by setting the leading δ coefficients of the $B(z^{-1},k)$ polynomial to zero.

The method of model identification employed in this paper comprises three stages [14]. In the first stage, the model structure and possible state dependent variables are identified by estimating a discrete-time linear transfer function model using any suitable method. The coefficient of determination [15] is employed here to determine the most appropriate model structure, and is defined,

$$R_T^2 = 1 - \frac{\sigma_e^2}{\sigma_y^2} \tag{3}$$

where σ_e^2 is the sample variance of the model residuals, that is, the difference between the model output and the actual output; and σ_y^2 is the variance of the actual output. If the variance of the model residuals is low compared with the variance of the actual output, R_T^2 tends to unity, indicating the model gives a good explanation of the actual output data. If the variances are similar in magnitude, R_T^2 tends to zero, indicating a poor fit.

During the second stage of model identification, stochastic time-varying parameter models are estimated using recursive Kalman filtering [16] and fixed-interval smoothing [17] algorithms. Since the variations in the parameters are functions of the state variables, the process can display severe non-linear or chaotic behaviour. Subsequently, these standard recursive estimation algorithms will not work satisfactorily. However, by sorting the data in a non-temporal order, for example, in ascending order so that the variations in the model parameters are slower and smoother, the standard identification methods can be used.

Equation (1) can be rewritten in the following vector-matrix form,

$$y_k = \boldsymbol{z}_k \boldsymbol{p}_k^{\mathrm{T}} + e_k \tag{4}$$

in which,

$$\begin{aligned} \boldsymbol{z}_k &= [-y_{k-1} \ldots -y_{k-n} u_{k-\delta} \ldots u_{k-m-\delta}] \\ \boldsymbol{p}_k &= [a_1(\chi_{11,k}) \ldots a_n(\chi_{1n,k}) b_0(\chi_{21,k}) \ldots b_m(\chi_{2m,k})] \end{aligned} \tag{5}$$

For convenience, $\boldsymbol{p}_k$ can be defined as,

$$\boldsymbol{p}_k = \left[p_{1,k} \;\; p_{2,k} \cdots p_{n+m+1,k}\right] \tag{6}$$

where $p_{i,k}$, $i = 1, 2, \ldots, n + m + 1$, relate to the model parameters $a_i(\chi_{1i,k})$ and $b_j(\chi_{2j,k})$. Each time-varying parameter is defined by the following stochastic state vector,

$$\boldsymbol{x}_{i,k} = \begin{bmatrix} l_k \\ s_k \end{bmatrix} \tag{7}$$

in which l_k and s_k are the changing level and slope of the parameter respectively.

The progression of the stochastic state vector can be described by a general random walk model,

$$\boldsymbol{x}_{i,k} = \boldsymbol{F}_i \boldsymbol{x}_{i,k-1} + \boldsymbol{g}_i \eta_{i,k} \tag{8}$$

where $\eta_{i,k}$ is zero mean white noise with variance q_i, and

$$\boldsymbol{F}_i = \begin{bmatrix} \alpha & \beta \\ 0 & \gamma \end{bmatrix}, \;\; \boldsymbol{g}_i = \begin{bmatrix} \psi \\ \omega \end{bmatrix} \tag{9}$$

The user-defined variables, $\alpha, \beta, \gamma, \psi$ and ω, are used to generate a family of random walks, including the scalar random walk $(\alpha = \psi = 1, \;\; \beta = \gamma = \omega = 0)$ and the integrated random walk $(\alpha = \beta = \gamma = \omega = 1, \;\; \psi = 0)$. The random walk model describes the evolution of the parameters over time and is a statistical mechanism allowing the parametric change to be estimated.

Combining (4) and (8) produces the following state-space equation,

$$\begin{aligned} \boldsymbol{x}_k &= \boldsymbol{F}\boldsymbol{x}_{k-1} + \boldsymbol{g}\eta_k \\ y_k &= \boldsymbol{H}_k \boldsymbol{x}_k + e_k \end{aligned} \tag{10}$$

where $\boldsymbol{x}_k$ is the state vector generated by concatenating the $\boldsymbol{x}_{i,k}$ state vectors; $\boldsymbol{H}_k$ is an observation vector obtained from $\boldsymbol{z}_k$; $\boldsymbol{F}$ is the state transition matrix that is a block diagonal aggregation of the $\boldsymbol{F}_i$ matrices; $\boldsymbol{g}$ is a concatenation of the $\boldsymbol{g}_i$ vectors; and $\boldsymbol{\eta}_k$ is a vector of zero mean white noise sequences with covariance $\boldsymbol{Q}$ that is independent of e_k. The noise variance ratio (NVR) matrix, $\boldsymbol{Q}_r$, is a diagonal matrix with a single NVR specified for each parameter, and is defined,

$$\boldsymbol{Q}_r = \frac{\boldsymbol{Q}}{\sigma^2} \tag{11}$$

The elements of the matrix $\boldsymbol{Q}_r$ and the parameters of the random walk model, or 'hyper-parameters', are estimated using a maximum likelihood approach with prediction error decomposition [18]. Increasing the NVR has the same effect as increasing the variance of the system noise in relation to the measurement noise, resulting in the error between the estimated output and the actual output having a larger effect on the parameter estimate. Note that sorting the data results in less variation between data steps, hence lower NVRs can be specified while still tracking the parameter variations, resulting in less noise propagation.

Since the DARX model has been formulated as a state-space model, a forward pass Kalman filter may be used in combination with a backward pass fixed-interval smoothing (FIS) algorithm to produce optimal parameter estimates. The backward pass FIS is required because the parameter estimates generated from the forward pass filtering are lagged. This recursive process continues until the forward pass estimates of the time-varying parameters no longer change significantly.

For the final identification stage, the resulting non-parametric estimate of each parameter is unsorted and plotted as a function of the variable upon which it depends, providing an indication of the location of any significant non-linearities. The non-parametrical estimates are then parameterised in terms of their associated dependent variable. In this paper, this is achieved by defining the parametric model as a polynomial function of the state variables, and the associated coefficients are obtained using standard numerical optimisation to minimise the error between the polynomial function and the non-parametric graph. The algorithm described in this section can be extended to multiple-input, single-output processes.

3. Wind turbine simulation

In this section, a computer simulation of a wind turbine and distribution grid has been created, incorporating grid and power electronic faults. A schematic of the simulation is shown in Fig. 2. The modelled turbine is a direct-drive and variable-speed pitch-controlled turbine with a multi-pole permanent magnet synchronous generator (PMSG) and fully rated voltage converter. This type of wind turbine requires no gearbox and is therefore appropriate

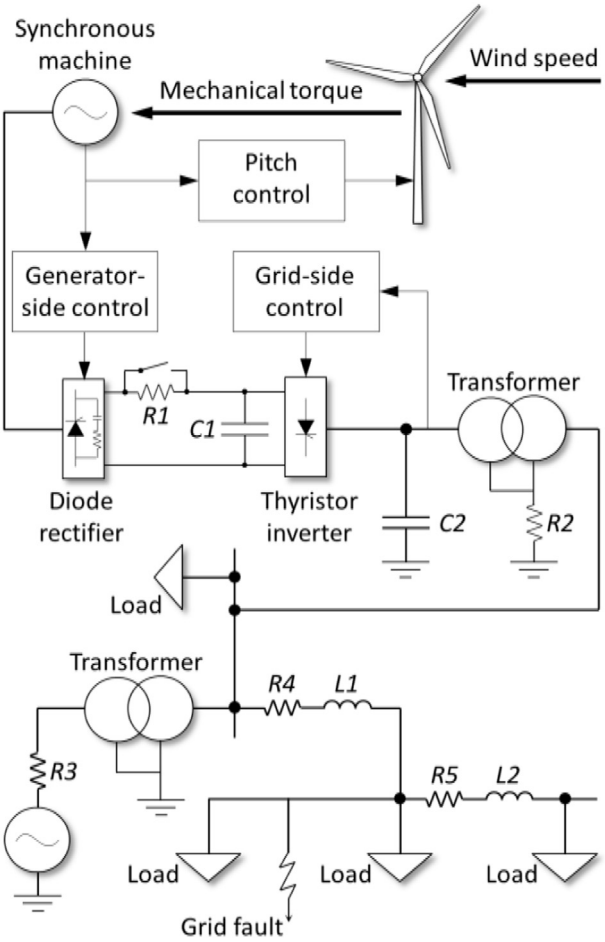

Fig. 2. Wind turbine and grid simulation, where $R1 = 1.1\ \Omega$, $R2 = 2\ \Omega$, $R3 = 0.1\ \mathrm{m}\Omega$, $R4 = R5 = 1\ \Omega$, $C1 = 2.3$ F, $C2 = 2$ mF, $L1 = L2 = 16$ mH.

for offshore applications, where it is essential for turbines to be low maintenance. In addition, the PMSG design is particularly suitable for large turbines generating power in the order of MW [19].

The modelled wind turbine has three blades, a rated power of 2 MW and a rated wind speed of 14 m/s; the output power of the turbine is regulated by adjusting the blade pitch. The turbine is coupled to a PMSG with 100 pole pairs and the grid connection is through an AC–DC–AC converter and a step-up transformer. Model parameters have been obtained from Ref. [20].

The AC–DC–AC converter is necessary in order to connect the variable voltage and frequency output from the generator to the fixed grid voltage and fixed 50 Hz grid frequency. The AC–DC–AC converter is composed of a generator-side diode rectifier, a DC bus with a storage capacitance, $C1$, and a grid-side six-pulse bridge thyristor inverter. Joule losses are limited by the inclusion of a switchable shunt resistor, $R1$. The transformer is required to step-up the voltage from 1.68 kV to 12.5 kV. A resistor, $R2$, is included to limit earth currents of the transformer during grid faults, and a capacitor, $C2$, is added to smooth output voltages.

The control system for PMSG-based turbines comprises three co-ordinated controllers [21,22]. The generator-side controller governs the operation of the generator and the power transferred from the generator to the DC link. This is achieved by adjusting the magnitude and angle of the voltage at the AC terminals of the converter and by regulating the speed of the generator. The grid-side controller maintains the DC link voltage at the reference value by exporting active power to the network, and allows the exchange of reactive power to the network as required. The network voltage is selected as the reference value, and the reference value for reactive power is set to zero for unity power factor operation. Finally, the pitch angle controller regulates the speed of the generator at high wind speeds. When the nominal generator power is reached, the pitch angle controller limits the rotor speed by adjusting both the pitch angle and its rate of change.

The grid is modelled as a radial distribution grid with a 34.5 kV, 300 MVA voltage source and a transformer to step-down the voltage to 12.5 kV. Asymmetrical and symmetrical grid faults can be incorporated in the grid.

The simulation has been built using PSCAD/EMTDC, a time domain simulation program for studying transient behaviour of complex electrical networks. The time step chosen for the simulation is 50 μs. The input to the simulation is wind speed, and this may take any form; for example, a constant, a random signal or a signal obtained from actual wind speed data.

3.1. Model identification

For model identification, a random signal is used as the wind speed input signal, with a mean speed of 14 m/s. In order to identify both faults on the distribution grid and power electronic faults, the RMS phase current and electrical torque are selected as the output variables.

For both the relationship between wind speed and phase current and the relationship between wind speed and electrical torque, it is assumed the numerator and denominator coefficients of the model are functions of the delayed input and the delayed output signals respectively.

3.2. Detection of grid faults

In order to demonstrate how grid faults can be detected with the identified non-linear models, typical asymmetrical and symmetrical faults such as AG (phase-A-to-ground), AB (phase-A-to-phase-B short circuit), ABG (phase-A-to-phase-B-to-ground) and ABCG (3-phase-to-ground) faults have been introduced individually into the simulation after 100 s, each lasting 0.2 s. An example of such a simulation, incorporating an AG fault, is shown in Fig. 3. The output of the simulation and the output predicted by the model are shown in the upper and middle subplots respectively. The lower subplot illustrates the residual signal, obtained by subtracting the predicted output from the actual output of the simulation. It is clear from this figure that the residual signal can be used to identify the occurrence of a grid fault. In addition, the magnitude of the residual signal gives an indication of the severity of the fault.

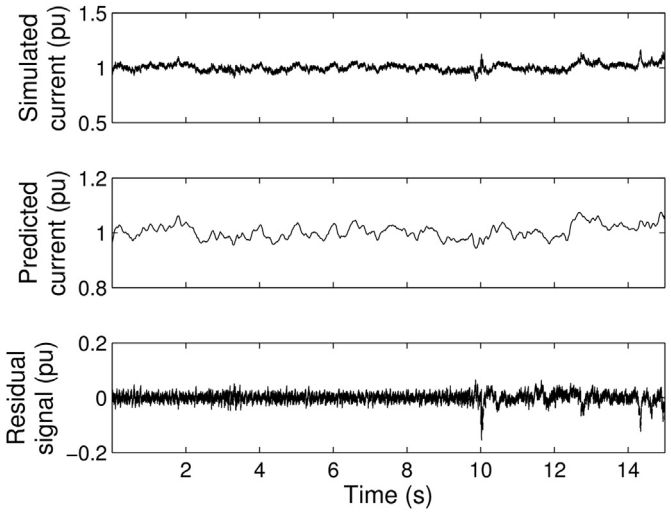

Fig. 3. Wind turbine simulation incorporating AG grid fault. Upper plot: simulated RMS phase current. Middle plot: model prediction. Lower plot: residual signal.

The model residuals for RMS phase current output during grid faults are summarised in Table 1. It can be seen the maximum positive residuals for the AG, AB and ABG faults are similar. However, the magnitude of the maximum negative residual can be used to distinguish between these fault types.

3.3. Detection of power electronics faults

In this section, power electronics faults are introduced into the simulation, specifically broken rotor bars and DC link capacitor faults. Rotor bar faults are associated with thermal and magnetic stresses caused by electromagnetic forces, residual stresses from manufacturing, and environmental stresses. This type of fault begins as high resistances in the rotor bars and can develop into cracks or holes [23]. DC link capacitors are required to endure high ripple currents leading to self-heating, which, in addition to high ambient operating temperatures, can result in the deterioration of the electrolyte material and the loss of electrolyte by vapour diffusion. The working life of a capacitor is also dependent upon operating voltage, current, and frequency. Consequently, DC link capacitors are considered one of the weakest components employed in power converters [24].

Rotor bar faults have been introduced into the simulation by adjusting the generator rotor phase resistances [25]. An example of

Table 1
Maximum residuals for RMS phase current for grid faults.

	AG fault	AB fault	ABG fault	ABCG fault
Maximum positive residual – current	0.065	0.067	0.062	0.196
Maximum negative residual – current	−0.154	−0.377	−0.248	−0.823

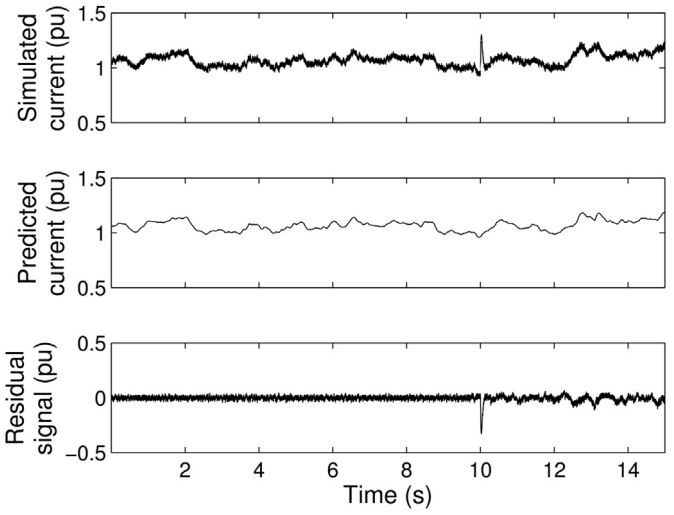

Fig. 4. Wind turbine simulation incorporating five broken bars. Upper plot: simulated RMS phase current. Middle plot: model prediction. Lower plot: residual signal.

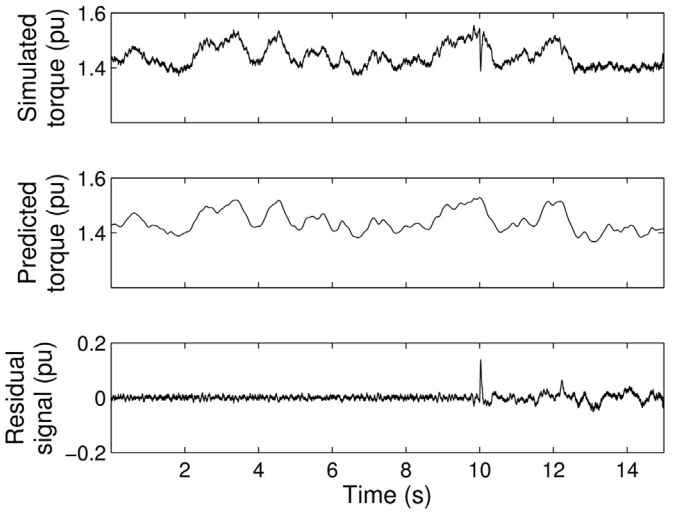

Fig. 5. Wind turbine simulation incorporating DC link capacitor fault. Upper plot: simulated electrical torque. Middle plot: model prediction. Lower plot: residual signal.

a simulation incorporating five broken bars is shown in Fig. 4, illustrating the phase current. The upper and middle subplots show the output of the simulation and the output predicted by the model respectively. The lower subplot illustrates the residual signal. As with the grid fault simulation, the faults occur after 100 s and last 0.2 s.

The model residuals for broken rotor bar faults are summarised in Table 2. The magnitude of the maximum negative residual for the phase current and the magnitude of the maximum positive residual for the electrical torque provide an indication of the severity of the fault.

An example of a simulation incorporating a faulty DC link capacitor operating at 90% of full capacity is shown in Fig. 5. The fault occurs after 100 s and lasts 0.2 s. The upper and middle subplots illustrate the simulated electrical torque output and the model prediction respectively, and the residual signal is shown in the lower plot.

The model residuals for the DC links capacitor faults are summarised in Table 3. The magnitude of the maximum negative residual for the phase current and the magnitude of the maximum positive residual for the electrical torque provide an indication of the severity of the fault.

It is worth mentioning that computer simulations of a wind turbine incorporating a doubly-fed induction generator (DFIG) with a grid connection have also been created by the authors [26]. The model has been built using SimPowerSystems, a plug-in for Mathworks' Simulink program. The system identification process is the same as outlined in Section 3.1. The model-based method described in Sections 3.2 and 3.3 has been used to detect grid and power electronic faults in the DFIG turbine model using the simulation data at a system level.

Table 2
Maximum residuals for RMS phase current and electrical torque for broken rotor bar faults.

	1 broken bar	2 broken bars	5 broken bars	10 broken bars
Maximum negative residual – current	−0.106	−0.163	−0.329	−0.442
Maximum positive residual – torque	0.066	0.139	0.255	0.338

4. SCADA data

Commercial wind farms usually employ a SCADA system, providing on-line information regarding various temperatures and pressures, power output, vibration, wind speed, and digital control signals. SCADA systems allow data to be acquired without the need to install additional instrumentation; therefore these data have been employed widely by researchers as the basis for CM systems [8,9].

In our research, the SCADA data are acquired from an operational wind farm, representing 16 months' operation. These data consist of 128 parameters, acquired at a sample rate in the order of 2 s, then processed and stored at 10 min intervals.

4.1. Model identification

SCADA data have been used to identify models describing the relationships between wind speed and the temperatures of the gearbox bearing and the generator winding. Gaps in SCADA data exist due to occasions when a wind turbine is inactive during periods of low and high wind speeds, and due to the occurrence of maintenance periods. Prior to model identification, it is necessary to remove these gaps when no power is generated.

In order to obtain generic 'reference turbine' models applicable to the entire wind farm, data from several turbines selected at random have been used for identification. Clearly, it is essential to obtain the reference turbine model by using only data acquired when the turbines are operating with no fault.

4.2. Detection of faults

A selection of power curves obtained from turbines operating on the wind farm is shown in Fig. 6, with the top subplot illustrating

Table 3
Maximum residuals for RMS phase current and electrical torque for DC link capacitor operating at a range of reduced capacities.

	97.5% Capacity	95% Capacity	90% Capacity	85% Capacity
Maximum negative residual – current	−0.661	−0.820	−1.09	−1.44
Maximum positive residual – torque	0.040	0.062	0.139	0.198

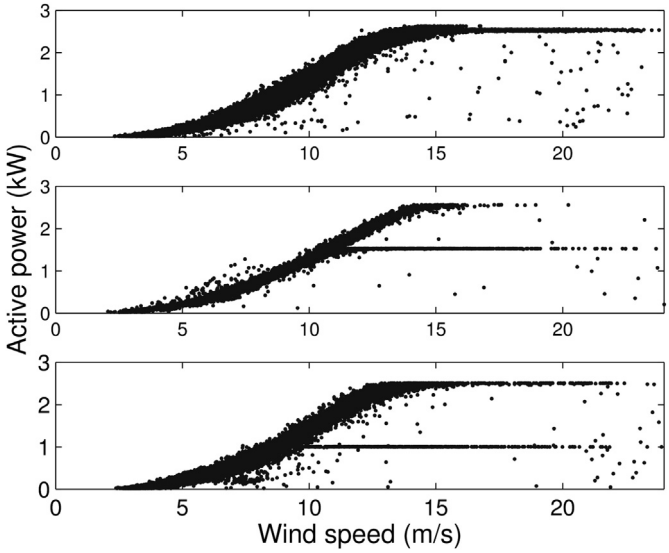

Fig. 6. Upper plot: power curve of reference turbine model. Middle and lower plots: power curves of turbines operating for a period with reduced power output.

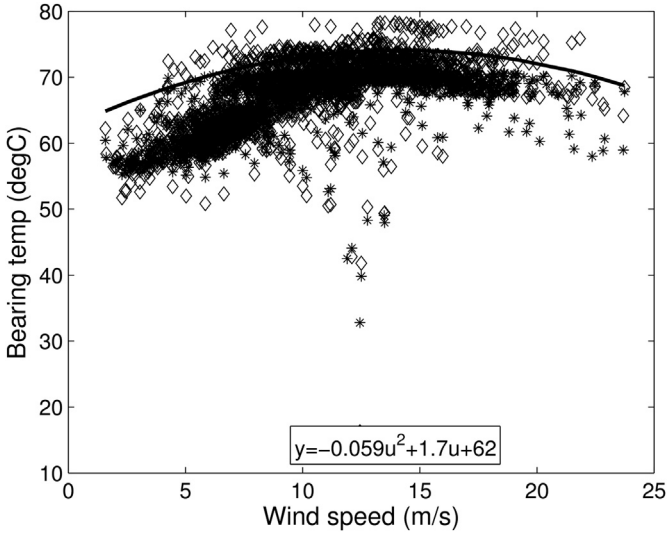

Fig. 8. Gearbox bearing temperature, *y*, as a function of wind speed, *u*. SCADA data (diamonds), model prediction (asterisks) and threshold (thick line) with defining equation.

the power output for the reference turbine model as a function of wind speed. The middle and lower plots of this figure show the power curves for two further turbines operating on the same wind farm. However, it can be seen that these turbines have, at some point, operated with a reduced power output following gearbox bearing and generator faults respectively.

In order to investigate whether the identified models are able to detect changes due to the onset of gearbox bearing and generator faults, the SCADA data acquired immediately before the occurrence of the faults have been compared with the corresponding output predicted by the reference turbine models, given wind speed as the input.

Considering initially the turbine associated with the gearbox fault illustrated in the middle subplot of Fig. 6, the output predicted by the reference gearbox model has been compared to the actual output of the turbine. The upper subplot of Fig. 7 illustrates the gearbox bearing temperature obtained from the SCADA data, and the middle subplot shows the bearing temperature predicted by the reference model. It can be seen from the residual signal illustrated in the lower plot that the temperature of the gearbox bearing deviates from the model prediction at hour 565, indicating the beginning of the bearing fault.

Fig. 8 shows the bearing temperature predicted by the model and the actual bearing temperature of the faulty turbine, as a function of wind speed. A curve, defined by the upper limit of output predicted by the SDP model, is also shown, together with its defining equation. The curve has been obtained using a function written in Matlab and represents a threshold level for the bearing temperature. This can be used as the basis of an early warning system, with an alarm raised when the threshold is exceeded.

Now considering the wind turbine associated with the generator fault illustrated in the bottom subplot of Fig. 6, the reference generator model prediction has been compared to the actual winding temperature of the turbine. The upper and middle subplots of Fig. 9 show the SCADA data and the reference model prediction respectively. The lower subplot illustrates the residual

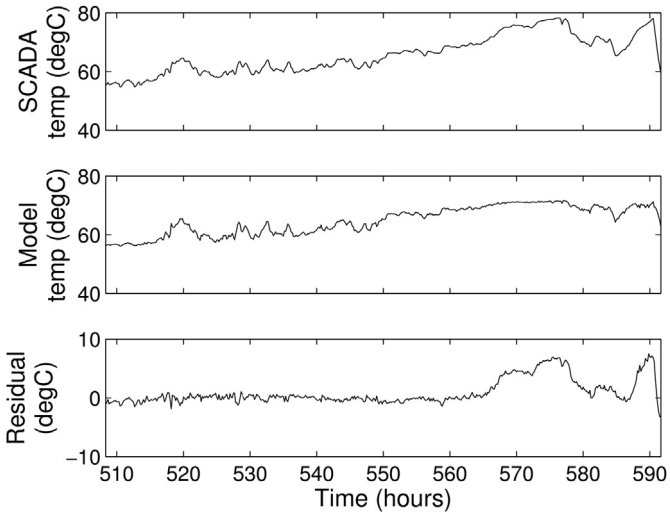

Fig. 7. Upper plot: gearbox bearing temperature from SCADA data. Middle plot: model prediction. Lower plot: residual signal.

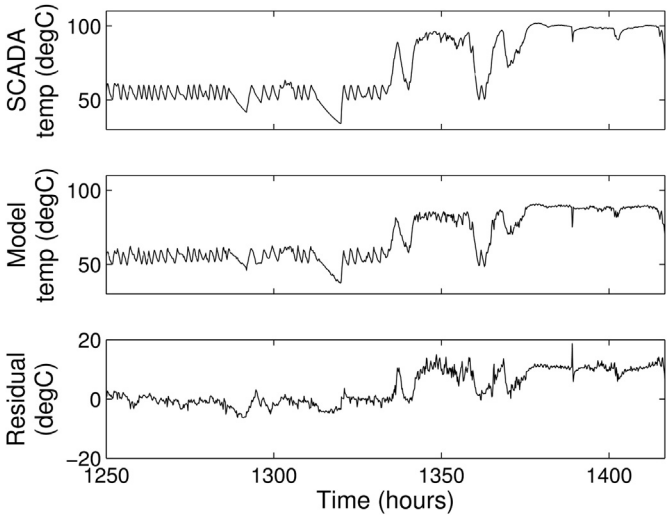

Fig. 9. Upper plot: generator winding temperature from SCADA data. Middle plot: model prediction. Lower plot: residual signal.

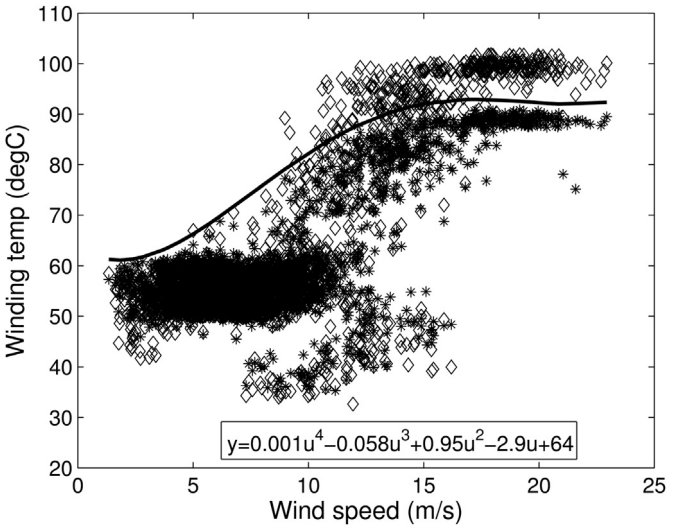

Fig. 10. Generator winding temperature, *y*, as a function of wind speed, *u*. SCADA data (diamonds), model prediction (asterisks) and threshold (thick line) with defining equation.

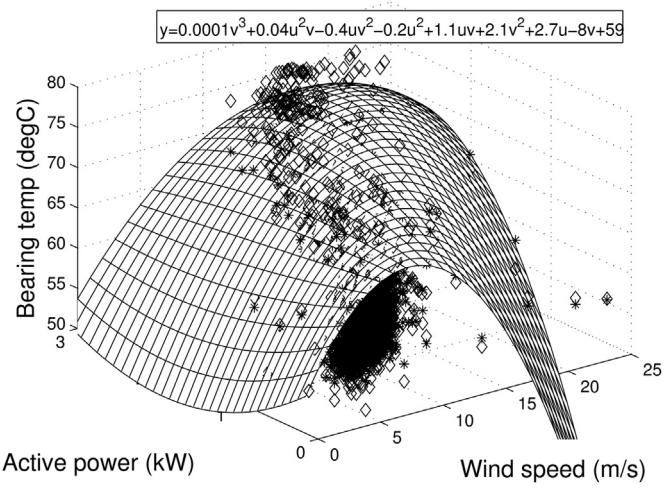

Fig. 12. Plot of gearbox bearing temperature, *y*, as a function of wind speed, *u*, and active power output, *v*. SCADA data (diamonds), model prediction (asterisks) and threshold (mesh) with defining equation.

signal. The residual signal shows that the actual temperature of the generator winding diverges from that predicted by the model at hour 1340, indicating the onset of the generator fault.

Fig. 10 illustrates the winding temperature predicted by the model and the actual output of the faulty turbine, as a function of wind speed. In a similar fashion to the gearbox model, a threshold can be obtained from the predicted output; the curve is defined by the equation also shown in Fig. 10.

The thresholds obtained for each of the parameters considered can be used as the basis of an early warning system, with an alarm raised when the threshold is exceeded. In order to avoid false alarms, the alarm will be raised only if the threshold is exceeded for a specified period.

4.3. Multivariate models

The temperatures of the gearbox bearing and generator winding depend not only upon the wind speed, but also the power output of the turbines. Consequently, this section considers the multivariate relationships between wind speed and active power output and the temperatures of the gearbox bearing and generator windings. These multivariate reference turbine models have been obtained using fault-free SCADA data as described in Section 4.1.

Considering again the turbine associated with the gearbox fault, the output predicted by the multivariate reference gearbox model has been compared to the SCADA data, as shown in Fig. 11. In a similar fashion to the single-input, single-output case, a three-dimensional surface has been obtained using the threshold function from the output predicted by the model as illustrated in Fig. 12. It is clear from this figure that the temperature of the bearing has exceeded that predicted by the SDP model on several occasions.

Fig. 13 shows the winding temperature obtained from the SCADA data acquired from the turbine associated with the generator winding fault. The model prediction is also shown in this figure. A corresponding threshold has been obtained from the predicted output, and is shown in Fig. 14. It is clear the winding temperature obtained from the SCADA data has exceeded the SDP model prediction on several occasions.

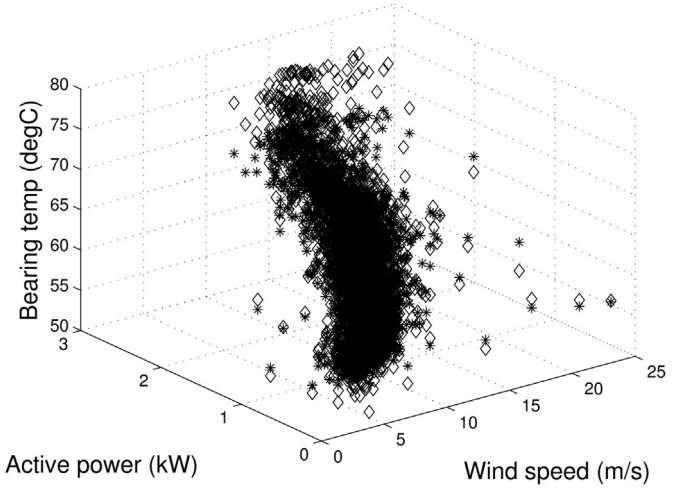

Fig. 11. 3D plot of gearbox bearing temperature as a function of wind speed and active power output. SCADA data (diamonds) and model prediction (asterisks).

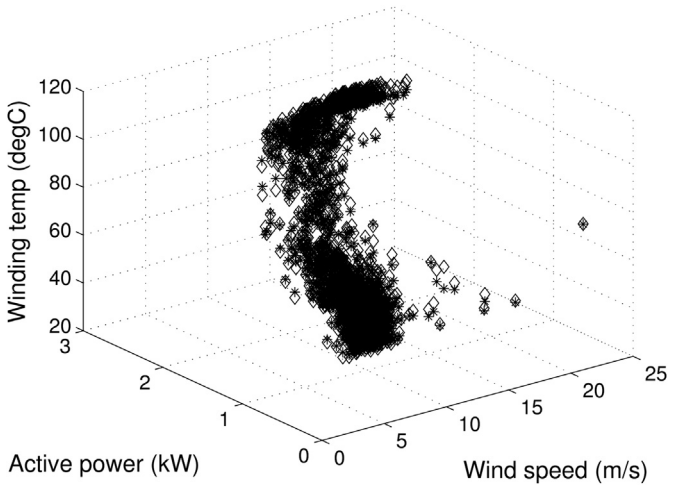

Fig. 13. 3D plot of winding temperature as a function of wind speed and active power output. SCADA data (diamonds) and model prediction (asterisks).

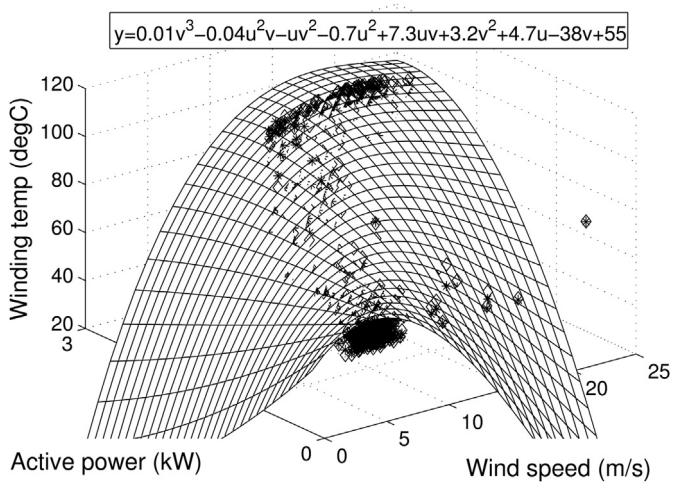

Fig. 14. 3D plot of winding temperature, *y*, as a function of wind speed, *u*, and active power output, *v*. SCADA data (diamonds), model prediction (asterisks) and threshold (mesh) with defining equation.

As with the single-input models, the threshold obtained from the multiple-input models can be used as the basis of an early warning system, with an alarm raised if the threshold is exceeded. This multivariate method provides more sensitive thresholds for the bearing and winding temperatures; a conventional method would derive the threshold purely on either wind speed or active power output.

5. FPGA implementation

It should be noted that the SCADA data employed in this paper are acquired at a sample rate of 10 min; clearly this leads to significant loss of data relating to the development of faults. Instead, condition monitoring systems normally gather high frequency and instantaneous data for analysis, and it is essential for the system to process these data in real-time.

A non-linear system can be described by a non-linear autoregressive function with exogenous inputs, in which the output signal is regressed on its delayed values together with the current and delayed values of the input signal [27],

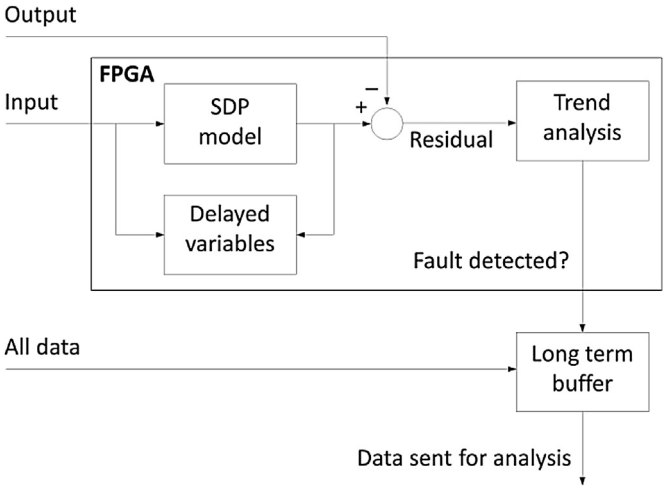

Fig. 15. Real-time implementation of proposed condition monitoring scheme.

$$y_k = f(y_{k-1}, y_{k-2}, \ldots, y_{k-n}, u_k, u_{k-1}, \ldots, u_{k-m}) \quad (12)$$

where y_k and u_k are defined as in (1). The function f can be approximated using an ANN in which connections between the neurons form a directed cycle, and feedback connections enclose several layers of the network, creating an internal state.

It should be noted that care needs to be taken to avoid 'over-fitting' of an ANN when the data are used to train the network, especially if input parameters are closely correlated [28]. Further, an ANN can become over-parameterised due to the complexity of the network [29]. Both over-fitting and over-parameterisation may lead to poor performance of the ANN when implemented on-line.

In contrast to ANN-based models, the method employed in this paper provides a parametrically efficient representation of non-linear processes, and, when implemented on-line, it is necessary only to store the current input signal and the delayed state variables together with the arithmetic expressions required to calculate the dependent parameters. Consequently, the SDP model-based CM scheme can be implemented straightforwardly in real-time using an FPGA, and Fig. 15 illustrates the proposed scheme.

FPGAs are in-system programmable, letting the user modify the operation of the device for dedicated applications. An FPGA allows deterministic execution of data processing tasks, and offers the ability to run multiple tasks concurrently. The FPGA employed in this research is a Xilinx Virtex-5 LX30, working at an operating clock frequency of 90 MHz. It employs 19,200 flip-flops, 19,200 look-up tables, and 1152 kbits of embedded RAM. The predicted output is calculated by the FPGA from the current input signal from the monitored component together with the delayed system variables and the polynomial function defining the parametric model. By monitoring the trend in the residual between the modelled output and the actual output based upon the adaptive threshold level, the system can determine if there is potential for a fault developing.

The complete CM scheme will also employ a long term buffer containing all data acquired from the monitoring system. If the system determines that there is a possible fault with the monitored component, data in this buffer will be sent to a control centre for analysis of the development of the fault. In this way, data transmission can be kept to a minimum.

The CM system has been implemented with reconfigurable data acquisition hardware. In this case, a National Instruments Compact RIO (cRIO), consisting of a control unit attached to an I/O chassis. Signals are generated by a dSPACE control board from either the output generated by the wind turbine simulation or using SCADA data. These signals are outputted in real-time at a sample rate of 5 kHz and then fed into analogue input modules housed in the I/O chassis. The Xilinx FPGA, embedded within the chassis, manages the signal acquisition and processing tasks. The cRIO hardware, including the FGPA, is programmed using LabVIEW. The hardware set-up is shown in Fig. 16, comprising (from left to right) the host computer, the cRIO control unit, the dSPACE control board, and an oscilloscope.

As an example, the SDP real-time implementation has been tested with the data obtained from the wind turbine with the bearing fault. The signals obtained from the FPGA, corresponding to the amount by which the adaptive threshold is exceeded and the period of time elapsed after the threshold is exceeded, are illustrated in Fig. 17. By monitoring these signals, it can be determined if there is potential for a fault developing. It is envisaged that this 'trend analysis' can be undertaken using, for example, a fuzzy logic-based inference system. However, this is beyond the scope of the paper.

Fig. 16. Reconfigurable hardware used to implement the proposed CM system.

6. Conclusions

This paper has presented a nonlinear data-based model-based methodology for condition monitoring (CM), demonstrated with data obtained from a computer simulation of a wind turbine and SCADA data acquired from an operational wind farm.

For the wind turbine simulation, it has been shown that the occurrence and severity of grid faults, broken rotor bars and DC capacitor faults can be identified using the output predicted by models of the relationships between wind speed and the RMS phase current and the electrical torque output.

Models obtained from SCADA data have been used to identify faults in the gearbox bearing and the generator winding. Adaptive thresholds for the gearbox bearing and winding temperatures have been obtained from the model prediction. In turn, these thresholds form the basis of a system that can provide an early warning of component failure and an indication of its severity. Further, the multivariate adaptive thresholds obtained in the paper are potentially more sensitive compared to conventional methods.

When implementing the nonlinear data-based models, it is necessary only to store the current input signal and the delayed system variables together with the arithmetic expressions required to calculate the dependent parameters. Consequently, it is relatively straightforward to implement the proposed model-based method on-line using a relatively low-powered processor, and the paper demonstrates a real-time implementation of the scheme using a field-programmable gate array and reconfigurable data acquisition hardware.

Future work will focus upon the development of the early warning system employing fuzzy logic to interpret the amount by which the adaptive threshold is exceeded and the period of time over which this occurs. In addition, the research will consider the number of data necessary to be retained in the long and short term buffers.

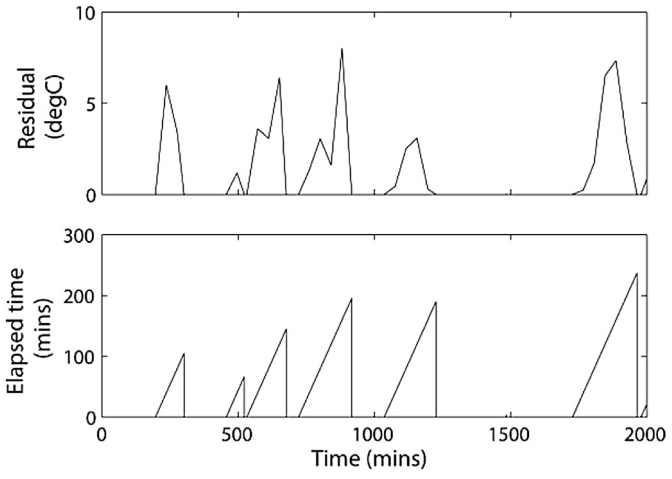

Fig. 17. Signals obtained from FPGA. Upper plot: amount by which the adaptive threshold is exceeded. Lower plot: time elapsed after threshold is exceeded.

Acknowledgements

The authors would like to thank the UK Engineering and Physical Sciences Research Council (EPSRC) for their funding support of the project under Grant EP/I037326/1. The permission of use SCADA data from Wind Prospect Ltd. is also gratefully acknowledged.

References

[1] Pepermans G, Driesen J, Haeseldonckx D, Belmans R, D'haeseleer W. Distributed generation: definition, benefits and issues. Energy Policy 2005;33:787–98.
[2] Ma X, Wang Y, Qin J. Generic model of a community-based microgrid integrating wind turbines, photovoltaics and CHP generations. Appl Energy 2013;112:1475–82.
[3] Jenkins N, Allan R, Crossley P, Kirschen D, Strbac G. Embedded generation. London, UK: IEE; 2000.
[4] Van Bussel GJW, Schöntag C. Operation and maintenance aspects of large offshore wind farms. In: European Wind Energy Conference, Dublin, Ireland; 1997.
[5] Communication Technologies Inc.. Supervisory control and data acquisition systems. USA: National Communications System; 2004.
[6] Dvorak D, Kuipers B. Model-based monitoring of dynamic systems. In: International Joint Conference on Artificial Intelligence, vol. 2; 1989. pp. 1238–43.
[7] Entezami M, Hillmansen S, Weston P, Papaelias MP. Fault detection and diagnosis within a wind turbine mechanical braking system using condition monitoring. Renew Energy 2012;47:175–82.
[8] Garlick WG, Dixon R, Watson SJ. A model-based approach to wind turbine condition monitoring using SCADA data. In: 20th International Conference on Systems Engineering, Coventry, UK; 2009.
[9] Schlechtingen M, Ferreira Santos I. Comparative analysis of neural network and regression based condition monitoring approaches for wind turbine fault detection. Mech Syst Signal Process 2011;25:1849–75.
[10] Üstüntaş T, Şahin AD. Wind turbine power curve estimation based on cluster center fuzzy logic modeling. J Wind Eng Ind Aerodyn 2008;96:611–20.
[11] Priestley MB. State-dependent models: a general approach to non-linear time series analysis. J Time Ser Anal 1980;1:47–71.
[12] Truong NV, Wang L, Wong PKC. Modelling and short-term forecasting of daily peak power demand in Victoria using two-dimensional wavelet based SDP models. Electr Power Energy Syst 2008;30:511–8.

[13] Gu J, Feng ZH, Ma X, Ni JF. Proportional-integral-plus control of robotic excavator arm utilising state-dependent parameter model. Appl Mech Mater 2011;48–49:1323–7.
[14] Young PC, McKenna P, Bruun J. Identification of nonlinear stochastic systems by state dependent parameter estimation. Int J Control 2001;74:1837–57.
[15] Steel RGD, Torrie JH. Principles and procedures of statistics. New York, USA: McGraw-Hill; 1960.
[16] Kalman RE. A new approach to linear filtering and prediction problems. J Basic Eng 1960;82:35–45.
[17] Bierman GJ. Fixed interval smoothing with discrete measurements. Int J Control 1973;18:65–75.
[18] Schweppe F. Evaluation of likelihood function for Gaussian signals. IEEE Trans Inf Theory 1965;11:61–70.
[19] Li H, Chen Z. Overview of different wind generator systems and their comparisons. Renew Power Gener 2008;2:123–38.
[20] CEDRAT, PSCAD Version 4.2. Wind turbine applications. Tech. paper KP05-A-EN-01/06; 2006.
[21] Hansen AD, Michalke G. Modelling and control of variable speed multi-pole permanent magnet synchronous generator wind turbine. Wind Energy 2008;11:537–54.
[22] Zhang D, Cross P, Ma X, Li W. Improved control of individual blade pitch for wind turbines. Sens Actuators A Phys 2013;198:8–14.
[23] Nandi S, Toliyat HA, Li X. Condition monitoring and fault diagnosis of electrical motors – a review. IEEE Trans Energy Convers 2005;20:719–29.
[24] Lee KW, Kim M, Yoon J, Lee SB, Yoo JY. Condition monitoring of DC-link electrolytic capacitors in adjustable-speed drives. IEEE Trans Ind Appl 2008;44:1606–13.
[25] Chen S, Živanovi&cacute R. Modelling and simulation of stator and rotor fault conditions in induction machines for testing fault diagnostic techniques. Eur Trans Electr Power 2010;20:611–29.
[26] Ma X, Cross P. A novel condition monitoring and real-time simulation system for wind turbines. In: European Wind Energy Conference and Exhibition, Vienna, Austria; 2013.
[27] Leontaritis IJ, Billings SA. Input-output parametric models for non-linear systems. Int J Control 1985;41:303–44.
[28] Cross P, Ma X. Feature selection for artificial neural network model-based condition monitoring of wind turbines. In: 10th International Conference on Condition Monitoring and Machinery Failure Prevention Technologies, Kraków, Poland; 2013.
[29] Hippert HS, Pedreira CE, Souza RC. Neural networks for short-term load forecasting: a review and evaluation. IEEE Trans Power Syst 2001;16:44–55.